A Re-entry Control Effectiveness Methodology for the Space Shuttle Orbiter

H. Ikawa*
Rockwell International, Downey, Calif.

An analytical methodology based on the Lees-Klineberg moment integral theory for two-dimensional, laminar, hypersonic viscous interaction has been developed to evaluate the aerodynamic control surface effectiveness of hypersonic winged vehicles, such as the Space Shuttle Orbiter, during high-angle-of-attack re-entry. A quasi-three-dimensional approach, i.e., a strip analysis of the vehicle planform, is used. Computed incremental aerodynamic coefficients produced by flap/elevon deflections of the Space Shuttle Orbiter correlate very favorably with wind-tunnel test data. Qualitative control effectiveness trends due to the effects of wall cooling, Reynolds number, and finite control surface chord length are discussed.

Nomenclature

a = speed of sound; also Klineberg velocity profile parameter

b = enthalpy profile parameter $-\{\partial/\partial\eta\,(S/S_w)\}_{\eta=0}$

C = constant in viscosity $(\mu/\mu_\infty)/(T/T_\infty)$

C_F = skin-friction coefficient $(\mu\partial u/\partial y)_w/\frac{1}{2}\rho_\infty u_\infty^2$

C_H = heat-transfer coefficient $(k\partial T/\partial y)_w/\rho_\infty(h_{0_e}-h_{0_w})$

$\bar{c}$ = orbiter reference length (474.8 in.)

C_N = normal force coefficient $N/\frac{1}{2}\rho_\infty u_\infty^2 S_{\text{ref}}$

C_m = pitching moment coefficient $M/\frac{1}{2}\rho_\infty u_\infty^2 \bar{c} S_{\text{ref}}$

$E = \frac{1}{\delta_i^*}\int_0^{\delta_i}\left(\frac{S}{S_w}\right)dY = \alpha(H_i)\,\sigma(b)$

$f = \left[2+\frac{\gamma+1}{\gamma-1}\,\frac{m_e}{1+m_e}\right]H_i + \frac{3\gamma-1}{\gamma-1}(1+ES_w) + \frac{M_e^2-1}{m_e(1+m_e)}Z$

$F = H_i + [(1+m_e)/m_e](1+S_wE)$

h_0 = total enthalpy

$H_i = \frac{1}{\delta_i^*}\int_0^{\delta_i}\frac{U}{U_e}\left[1-\frac{U}{U_e}\right]dY$

$J = \frac{1}{\delta_i^*}\int_0^{\delta_i}\frac{U}{U_e}\left[1-\left(\frac{U}{U_e}\right)^2\right]dY$

k = thermal conductivity

$K = \beta C M_\infty/M_e\delta_i^* Re_{\delta_i^*}$

l = surface length

$m = [(\gamma-1)/2]M^2$

M = Mach number; also pitching moment

N = normal force

p = static pressure

$P = \delta_i^*\left[\frac{\partial}{\partial Y}\left(\frac{U}{U_e}\right)\right]_{Y=0}$

Pr = Prandtl number

$Q = -\delta_i^*\left[\frac{\partial}{\partial Y}\left(\frac{S}{S_w}\right)\right]_{Y=0} = b/\alpha(H_i)$

$R = 2\delta_i^*\int_0^{\delta_i}\left[\frac{\partial}{\partial Y}\left(\frac{U}{U_e}\right)\right]^2 dY$

Re_x = Reynolds number $a_\infty M_\infty x/\nu_\infty$

$Re_{\delta_i^*}$ = Reynolds number $a_\infty M_\infty \delta_i^*/\nu_\infty$

S = total enthalpy function $h_0/h_{0_e}-1$

S_{ref} = Orbiter reference area (2690 ft^2)

$T = \int_0^{(\eta)\,U/U_e=0.99}\left[\frac{U}{U_e}\,\frac{S}{S_w}\right]d\eta$; also static temperature

$T^* = \frac{1}{\delta_i^*}\int_0^{\delta_i}\left[\frac{U}{U_e}\,\frac{S}{S_w}\right]dY = \alpha(H_i)\,T(H_i,b)$

u,v = velocity components

U,V = Stewartson-Illingworth transformed velocity components

x,y = curvilinear coordinates

X,Y = Stewartson-Illingworth transformed coordinates

$Z = \frac{1}{\delta_i^*}\int_0^{\delta_i}\frac{U}{U_e}dY$

$\alpha = \left[\int_0^{(\eta)\,U/U_e=0.99}\left(1-\frac{U}{U_e}\right)d\eta\right]^{-1}$; also angle of attack

α_w = surface deflection angle ($\alpha_w<0$ compression)

β = $a_e p_e/a_\infty p_\infty$

γ = ratio of specific heats

δ = boundary-layer thickness

δ_i = transformed boundary-layer thickness $\int_0^{(Y)\,U/U_e=0.99}dY$

δ_u = boundary-layer velocity thickness

δ^* = boundary-layer displacement thickness

δ_i^* = transformed boundary-layer displacement thickness $\int_0^{\delta_i}\left[1-\frac{U}{U_e}\right]dY$

η = Cohen-Reshotko similarity variable

Θ = local streamline inclination at edge of boundary layer

θ = boundary-layer momentum thickness

θ^* = boundary-layer mechanical energy thickness

θ^{**} = boundary-layer energy thickness

μ = viscosity coefficient

ρ = gas density

$\bar{\chi}$ = hypersonic viscous interaction parameter $M_\infty^3 C^{1/2}/(Re_x)^{1/2}$

Subscripts

B = Blasius values

BF = body flap

CG = Orbiter center of gravity (0.65 LB)

e = local flow outside boundary layer (external); also elevon

Received Jan. 17, 1977; presented as Paper 77-6 at the AIAA 15th Aerospace Sciences Meeting, Los Angeles, Calif., Jan. 24-26, 1977; revision received Aug. 15, 1977.

Index categories: Supersonic and Hypersonic Flow; Jets, Wakes, and Viscid-Inviscid Flow Interactions.

*Member of Technical Staff. Member AIAA.

F = flap; elevon; deflection surface
HL = corner of flat-plate or wedge (hinge line)
i = transformed (incompressible)
L = local unperturbed properties outside of boundary layer
LB = Orbiter body length (1290 in.)
R = reattachment point
S = separation point
SI = strong interaction
TE = trailing edge
w = wall (surface); also forewing
WI = weak interaction
∞ = freestream condition

Introduction

THE importance of understanding hypersonic laminar flow separation problems produced by compressively deflected surfaces has been revived recently due to the development of the Space Shuttle Orbiter. The large deflections of control surfaces (flap/elevon) required to attain hypersonic vehicle trim and control during re-entry induce adverse pressure gradients within the boundary layer. Consequently, the laminar boundary layer separates, causing a loss in control surface effectiveness. The existence of the flow separation phenomenon, due to the viscous-inviscid flow interaction, has been known for quite some time. Theoretical and experimental investigations of this flow phenomenon have been pursued by many investigators,[1-10] primarily for academic interest, since no urgent application for vehicle design existed until stability and control problems associated with high-angle-of-attack re-entry conditions were surfaced during Space Shuttle Orbiter wind-tunnel tests.[11]

Three-dimensional flow separation prediction programs and valid theoretical methods to investigate vehicle control effectiveness due to viscous interaction do not exist. These programs are necessary, for example, to extend wind-tunnel test data to the full-scale flight conditions (i.e., scaling effects). Two-dimensional finite-difference and moment integral techniques[1-10] are usually too sophisticated and/or uneconomical for engineering applications, such as vehicle design; therefore, empirical approaches[12,13] are employed. However, these methods do not always offer a satisfactory solution. For example, inability to predict the reattachment point on short finite-length flaps results in nonconvergence of the solution. An attempt to solve exact three-dimensional viscous-inviscid interaction problems by finite-difference techniques is an enormous task, and the cost of computer operations is prohibitive for engineering applications.

In order to alleviate these problems, a quasi-three-dimensional prediction methodology, based on the two-dimensional Lees-Klineberg moment integral theory[1,2] and the strip analysis, was developed for investigation of hypersonic laminar flow separation (ideal gas) and static stability and control of winged re-entry vehicles, such as the Space Shuttle Orbiter. Description of the theory, technical approach for solving the stability and control of the Space Shuttle Orbiter during high-angle-of-attack re-entry, and factors that influence the aerodynamic performance of control surfaces will be discussed.

Governing Equation

The governing equations that describe the steady, two-dimensional, laminar viscous interaction of ideal gas flow are expressed in integral equation form of the compressible laminar boundary layer as given by Klineberg[1]:

$$\frac{d\delta^*}{dx} - (\delta - \delta^*)\frac{d\ell n \rho_e u_e}{dx} = \frac{v_e}{u_e} = \tan\Theta \tag{1}$$

$$\frac{d(\rho_e u_e^2 \theta)}{dx} + \delta^* \rho_e u_e \frac{du_e}{dx} = \left[\mu \frac{\partial u}{\partial y}\right]_w \tag{2}$$

$$\frac{d(\rho_e u_e^3 \theta^*)}{dx} + 2(\delta^* - \delta_u)\rho_e u_e^2 \frac{du_e}{dx} = 2\int_0^\delta \mu \left[\frac{\partial u}{\partial y}\right]^2 dy \tag{3}$$

$$\frac{d(\rho_e u_e \theta^{**})}{dx} = -\left[\frac{\mu}{Pr}\frac{\partial}{\partial y}\left(\frac{h_0}{h_{0_e}}\right)\right]_w \tag{4}$$

The compressible boundary-layer equation can be transformed into the equivalent incompressible form by assuming the Chapman-Rubesin viscosity law,[14] $\mu/\mu_\infty = C(T/T_\infty)$, and by using the Stewartson transformation[15]:

$$dX = C\frac{a_e p_e}{a_\infty p_\infty}dx \qquad dY = \frac{a_e \rho}{a_\infty \rho_\infty}dy \qquad U = \frac{a_\infty}{a_e}u$$

The flow property relationships in the attached and separated boundary layer are assumed to be described by the form factor H_i and the total enthalpy profile parameter b. With these assumptions, Eqs. (1-4) can be transformed into the following:

$$F\frac{d\ell n \delta_i^*}{dx} + \left[1 + \frac{1+m_e}{m_e} S_w \frac{\partial E}{\partial H_i}\right]\frac{dH_i}{dx} + \frac{1+m_e}{m_e} S_w \frac{\partial E}{\partial b}\frac{db}{dx} - \left[F + \frac{Z}{m_e}\right]\frac{d\ell n p_{e_t}}{dx} + f\frac{d\ell n M_e}{dx} = \frac{\beta}{m_e}\frac{(1+m_e)}{(1+m_\infty)\delta_i^*}\tan\Theta - ES_w\frac{1+m_e}{m_e}\frac{d\ell n S_w}{dx} \tag{5}$$

$$H_i\frac{d\ell n \delta_i^*}{dx} + \frac{dH_i}{dx} + [2H_i + 1 + ES_w]\frac{d\ell n M_e}{dx} = KP \tag{6}$$

$$J\frac{d\ell n \delta_i^*}{dx} + \frac{dJ}{dH_i}\frac{dH_i}{dx} + [3J + 2T^* S_w]\frac{d\ell n M_e}{dx} = KR \tag{7}$$

$$T^*\frac{d\ell n \delta_i^*}{dx} + \frac{\partial T^*}{\partial H_i}\frac{dH_i}{dx} + \frac{\partial T^*}{\partial b}\frac{db}{dx} + T^*\frac{d\ell n M_e}{dx} = \frac{KQ}{Pr_w} - T^*\frac{d\ell n S_w}{dx} \tag{8}$$

The continuity equation [Eq. (5)] provides the coupling between the displaced boundary layer and external inviscid flow. The wall cooling parameter S_w appears explicitly and can be selected arbitrarily. The wall temperature gradient term also appears explicitly in the continuity and energy equations. The entropy gradient influence introduced by the curved bow shock is included in the continity equation. Entropy and wall temperature gradient effects, however, are not presently coded in the computer program.

Velocity and Total Enthalpy Profile Parameters

The profile quantities required for the moment integral method depend on both the velocity and the total enthalpy distributions through the viscous layer. These relationships are obtained from the similarity solutions of Cohen and Reshotko[16] for both forward and reverse flows. The universal flow profile quantities generated by Klineberg in terms of the velocity profile parameter a are redefined and represented by polynomial relationships in terms of a form factor H_i and the wall enthalpy parameter b. Similar profile parameters presented by Georgeff[10] do not describe the large separated region (i.e., $H_i < 0.10$, $b < 0.05$); therefore, parameters describing large separated regions have been generated in polynomial form.

Inviscid Stream and Viscous Layer Interaction

For two-dimensional supersonic inviscid flow, changes in Mach number are determined entirely by the local streamline inclination. For viscous interaction flow, the local Mach number $M_e(x)$ at the edge of the boundary layer is related to the induced streamline angle Θ, which can be defined by the appropriate inviscid solution of the external flowfield. The slowly growing nature of the boundary layer, acting as a blanket over the surface of the abrupt discontinuity, allows the assumption of isentropic compression near the wall. Hence Θ can be represented by the Prandtl-Meyer solution:

$$\Theta = \nu(M_\infty) - \nu(M_e) - \alpha_w + dt/dx \tag{9a}$$

$$\nu(M) = \sqrt{\frac{\gamma+1}{\gamma-1}} \arctan \sqrt{\frac{\gamma-1}{\gamma+1}(M^2-1)} - \arctan\sqrt{M^2-1} \tag{9b}$$

where $\alpha_w < 0$ represents the compression surface, and dt/dx represents the surface slope generated by the wing section thickness and/or camber distributions.

Boundary Conditions

Separation and the reattachment points of the viscous interaction flowfield are unknown a priori and are determined as the solution of a given problem. The required boundary conditions to be satisfied are as follows:

1) The condition to be satisfied just upstream of the interaction region x_1 (see Fig. 1) and ahead of the compression ramp is determined from among a Blasius, weak interaction, or strong interaction leading-edge solution, depending upon the value of hypersonoc interaction parameter $\bar{\chi}$.

2) Two types of downstream boundary conditions exist. For finite-length flaps or ramps, flow expands rapidly around the trailing edge but with finite boundary-layer thickness and Mach number. However, for the flow over a highly cooled surface, the Crocco-Lees critical point may appear on the flap/elevon between the reattachment point and the trailing edge. In this case, smooth transition of the solution at the critical point is sought, and rapid expansion of the flow at the trailing edge is ignored. For the infinite-length ramp, the final solution approaches Blasius' condition, with the derivatives of the edge Mach number and form factor going to zero. ($d\ell nM_e/dx$, $dH_i/dx \to 0$).

Computational Scheme

Lees-Klineberg Moment Integral Theory

A separated flowfield is depicted schematically in Fig. 1. The initial perturbation of the upstream flow is a growth of the boundary layer induced by the adverse pressure gradient generated by the compressibly deflected surface. It occurs at a point x_1, which is selected arbitrarily to initiate the computation. The fourth-order Runge-Kutta method is used to integrate the set of differential equations in the downstream direction. Location of x_1 is iterated until the downstream boundary conditions on the ramp are satisfied.

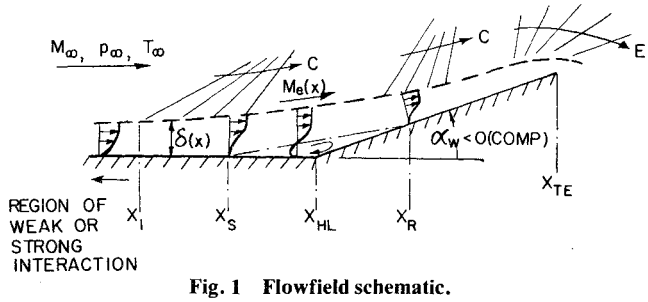

Fig. 1 Flowfield schematic.

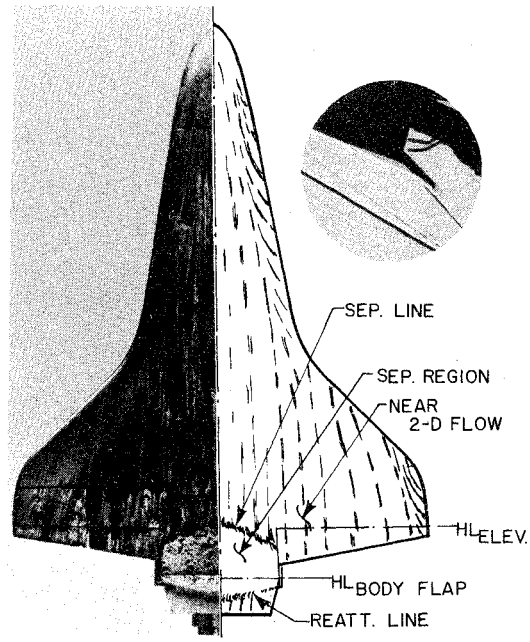

Fig. 2 Orbiter oil flow photograph showing body flap flow separation ($M_\infty = 6$, CF_4, $\alpha = 25$ deg, $\delta_e = 0$, $\delta_{BF} = 22.5$ deg, $Re_{LB} = 0.16 \times 10^5$).

For flow over a highly cooled nonadiabatic wall, a mathematical singularity appears near x_1. In the previous methodoligies,[1-3,10] a discontinuous sudden jump in the fluxes of mass, momentum, and mechanical energy is allowed at the separation point to pass through the singular point, which is required to satisfy the conservation law. However, the viscous interaction initiates a smooth isentropic compression at the point x_1, a few boundary layer thicknesses upstream of the separation point, for both adiabatic and nonadiabatic flows. In the present approach, small perturbations in the parameters H_i and b are allowed and are iterated in addition to the x_1 location until a smooth heat-transfer rate transition and stable downstrem integration are achieved to overcome the mathematical singularity.

Prediction of Shuttle Orbiter Hypersonic Control during Re-entry

In order to predict the realistic Orbiter aerodynamic performance, the following computational schemes are used. The moment integral theory is extended to include the effects of finite flap/elevon chord lengths and small surface perturbations from the flat plate by considering the thickness/camber distribution of a wing section. The effect of angles of attack are considered by using the local flow properties existing on the windward side of the vehicle. Experimental data indicate that the measured pressure on the windward surface downstream of the wing leading edge approaches the tangent cone value. Therefore, the Shuttle Orbiter analysis is unique in that the flowfield that contributes to flow separation is based on a Mach number range of low supersonic to low hypersonic speeds ($1.2 \le M \le 6.0$) and is not associated directly with high re-entry freestream Mach number ($10 \le M_\infty \le 25$).

The oil flow photograph of Fig. 2† shows that the windward flow direction of a high-angle-of-attack hypersonic reentry vehicle is nearly two-dimensional, except near the leading edge and the tips of wing. The airstream approaching the elevon/body flap is interacting perpendicularly with the unswept hinge lines. A large separated region produced by the body flap deflection shows some three-dimensional patterns, as observed in the bow-shaped separation and reattachment lines. These are produced by the flow spillage along the

†Courtesy of NASA Langley Research Center.

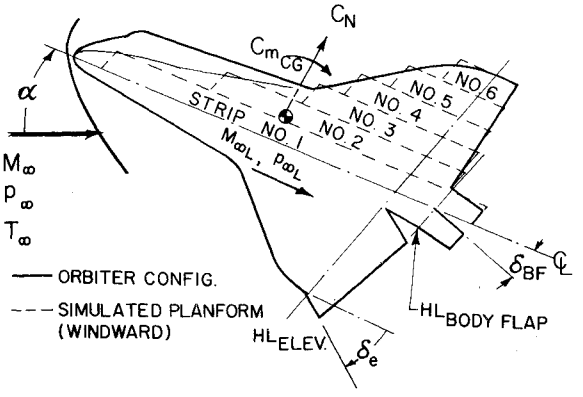

Fig. 3 Quasi-three-dimensional simulation.

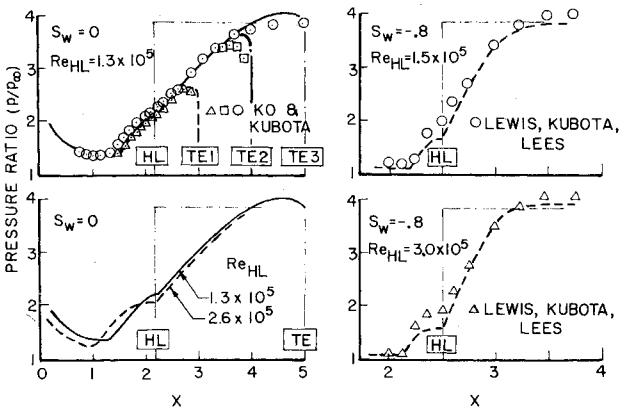

Fig. 4 Pressure distribution comparisons for two-dimensional flow ($M_\infty = 6.0, \gamma = 1,4, \alpha_w = -10.5$ deg).

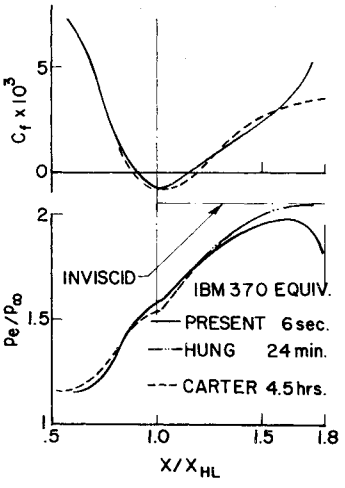

Fig. 5 Numerical result comparisons for two-dimensional flow ($M_\infty = 3.0$, $\gamma = 1.4$, $S_w = 0.0$, $\alpha_w = -10$ deg, $Re_{HL} = 16{,}800$); present result, finite length flap; Hung and Carter, infinite length flap.

spanwise edges which tends to reduce the separated region. However, the effects of flow spillage and crossflow component normally associated with the three-dimensional voscous interaction problems are minimized by the deflected surface having an *unswept hinge line*. Therefore the gross effects of the Space Shuttle Orbiter control surface effectiveness problem can be analyzed by the quasi-three-dimensional approach with reasonable accuracy, even though the microscopic flowfield detail may be highly three-dimensional.

A following quasi-three-dimensional scheme is used to simulate the Orbiter configuration in the computation. Since the Reynolds number of the corner (Re_{HL}) which dictates the flow separation mechanism is proportional to the running length of the forewing section from the leading edge to the hinge line, the three-dimensionality of the Orbiter wing is represented by several two-dimensional strips having the local spanwise chord length of the Orbiter planform (Fig. 3). Consequently, the effects of spanwise variations in local distributions of pressure, shear stress, and aeroheating rate are taken into account. Although a limitation of the present method is to neglect strip-to-strip interaction and spanwise edge effects due to flow spillage, the present assumptions produce acceptable results. The validity of the present technique has been verified by comparing the predicted results with Space Shuttle Orbiter wind-tunnel test data.

Results and Discussions

Verification of Moment Integral Theory

The accuracy is illustrated in Figs. 4-6. Computations were made with the two-dimensional laminar flow separation computer program for the case where $M_\infty = 6.0$ flow occurs over a finite-length flap deflected 10.5 deg. Agreement with wind-tunnel data taken by Ko and Kubota is excellent for the adiabatic wall case (left-hand side of Fig. 4). The importance of the flap finite chord length is also demonstrated in this figure. Peak pressure levels predicted by the inviscid flow theory are never achieved with the presence of laminar viscous interaction on the short flap if its trailing edge terminates in the region where ideal viscous interaction pressure recovery is occurring. Pressure distributions computed for the nonadiabatic, highly cooled wall ($S_w = -0.8$) are compared with expreiments of Lewis et al.[18] Agreement is good except near the pressure plateau on the separated region, as shown on the right-hand side of Fig. 4. The computations show that no finite flap length effects appear because full pressure recovery was attained for the shortest flap used in the computation. However, if the flap length is shortened further, qualitatively the same trend as the adiabatic case should be observed for the nonadiabatic flow separation case. A rapid pressure recovery and a smaller separated region result for the flow over the very cooled wall. Both adiabatic and nonadiabatic cases have shown that the upstream propagation of the separated region occurs with increasing Reynolds number in the laminar flow region.

Results computed with the present program and the more sophisticated finite-difference technique[8,9] are compared in Fig. 5. The flow conditions used in this computation are $M_\infty = 3.0$, $Re_{HL} = 1.68 \times 10^4$, $\gamma = 1.4$, $\alpha_w = -10$ deg, and $S_w = 0$ (adiabatic wall). The present computation is conducted on a flat plate with a finite-length flap, which shows the flow expansion effects around the trailing edge taken at $x_{TE}/x_{HL} = 1.8$. The computations of Hung and Carter were based on an infinite-length ramp. The significant feature is the comparison of representative computational times. The computational speed of the IBM 370 is almost two times as fast as the CDC 6600 but approximately one-half the speed of the CDC 7600.[17] If the required computational times of these computers are converted to equivalent IBM 370 times, the sample problem can be solved in less than 6 sec by the present program, 24 minutes for the Hung[8] (12 min on CDC 7600), and 3 to 4.5 hr for the Carter[9] (5.5 to 9 hr on CDC 6600) programs. It can be seen that very substantial savings in computational time with little sacrifice in accuracy is realized with the present program (i.e., approximately 200 cases can be analyzed with the present compared to a single case using Hung's program).

The effect of wall cooling is compared with the experimental data of Bloy and Georgeff[19] (Fig. 6). The test flow conditions were $M_\infty = 12.2$, $Re_{HL} = 5.2 \times 10^5$, $S_w = -0.78$, and for deflection angles of 8, 10, and 12 deg. The predicted pressure and aeroheating rate distributions (dashed lines) show better agreement with test data than previously developed methods,[19] giving further credence to the present methodology.

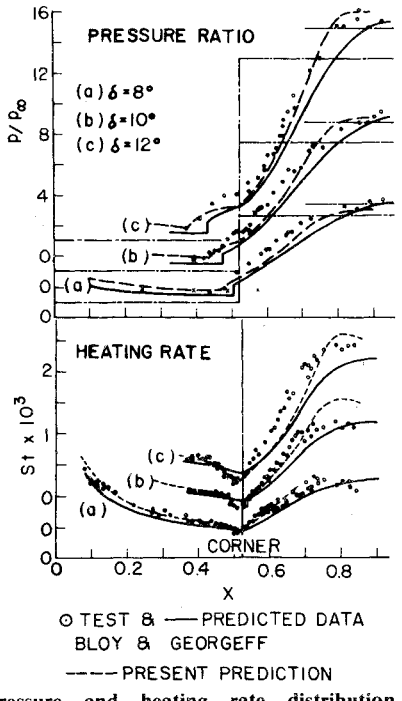

Fig. 6 Pressure and heating rate distribution comparisons ($M_\infty = 12.2, \gamma = 1.4, S_w = -0.78, Re_{HL} = 5.2 \times 10^5$).

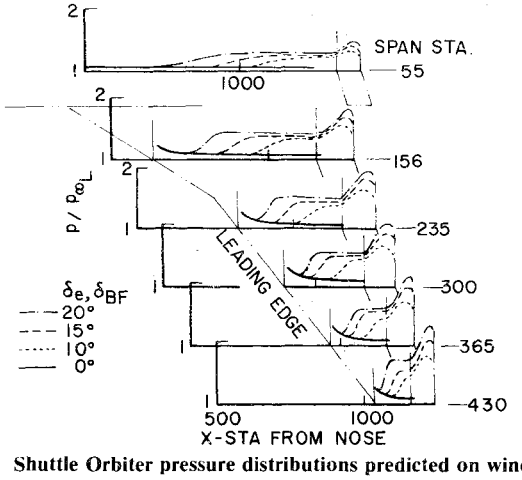

Fig. 7 Shuttle Orbiter pressure distributions predicted on windward surface ($M_\infty = 22$, $\alpha = 30$ deg, $\gamma = 1.4$, $S_w = 0$, $M_\infty = 2.95$, $p_{\infty L}/p_\infty = 207.6$, $Re_{LB} = 4.8 \times 10^5$).

Verification of Quasi-Three-Dimensional Approach

The next step is to validate the quasi-three-dimensional technique for analysis of the control surface effectiveness of hypseronic winged vehicles. This task will be accomplished by comparison between predicted and wind-tunnel test data of the Space Shuttle Orbiter.

For a freestream Mach number of 22 and angle of attack of 30 deg, the local inviscid Mach number ($M_{\infty L}$) is 2.95 on the vehicle windward side. Predicted pressure distributions for control surface deflections (δ_e, δ_{BF}) of 10, 15, and 20 deg for the adiabatic wall case are shown in Fig. 7. The upstream propagation of the separated region due to increasing surface deflection and quasi-three-dimensional effects (variation of separated regions and peak pressures) is observed. Unfortunately, experimental pressure distribution data for the Shuttle Orbiter are unavailable for comparison.

The longitudinal and spanwise integration of pressure distributions, as shown in Fig. 7, produce the normal force and pitching moment acting on the vehicle. Static stability and control data are compared in Fig. 8. Here the increments in

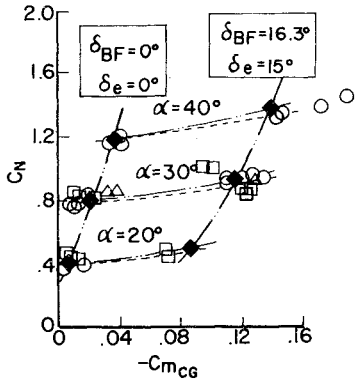

Fig. 8 Shuttle Orbiter stability and control.

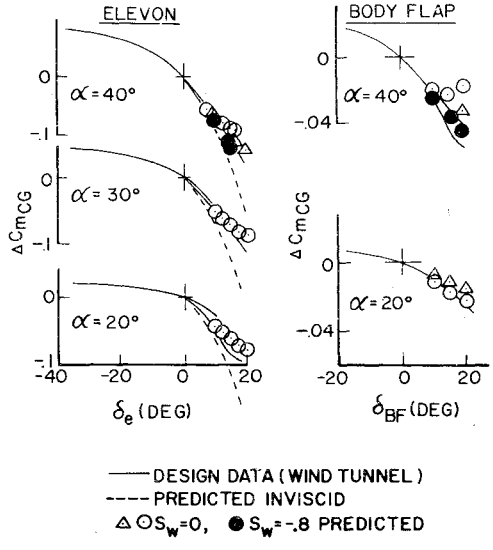

Fig. 9 Shuttle Orbiter incremental pitching moment comparisons.

predicted force and moment coefficients produced by control surface deflections (i.e., $\Delta C = C_{\delta \neq 0} - C_{\delta = 0}$) are added to the experimental data for no surface deflections for each of the three values of angle of attack. Although absolute force and moment coefficients predicted by the present method do not agree well with experimental values, the increments due to control surface deflections show very good agreement.

Incremental pitching moment coefficients plotted against elevon and body flap deflections are compared in Fig. 9. Data presented in Ref. 11 which were obtained from compilation of experimental data are shown as solid lines. These lines define the max-min range. The computed results are shown as data points. Considering the range of experimental data scatter as observed in Fig. 8, the agreement is excellent. Incremental pitching moments computed for inviscid flow (two-dimensional oblique shock theory) are shown as dashed lines. (Note: considerable deterioration in the control effectiveness results because of the presence of the viscous-inviscid flow interactions).

Reynolds Number Effects

The hypersonic boundary-layer growth on a flat-plate surface and its interaction with the inviscid flowfield are enhanced with increasing hypersonic similarity parameter $\bar{\chi}$ (i.e., increase in Mach number and/or decrease in Reynolds number). The control surface effectiveness is also highly influenced by the nature of the oncoming boundary layer.

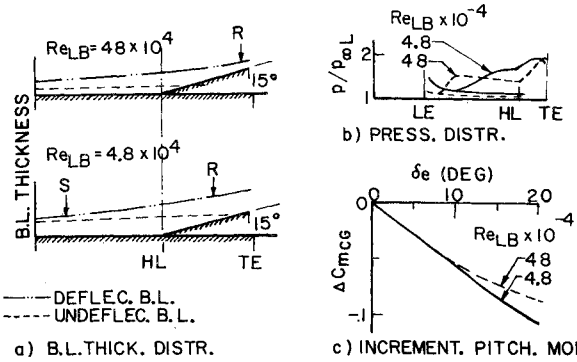

Fig. 10 Effects of elevon effectiveness on Reynolds number ($M_\infty = 22$, $\alpha = 40$ deg, $M_{\infty L} = 1.8$, $\gamma = 1{,}4$, $S_w = 0$).

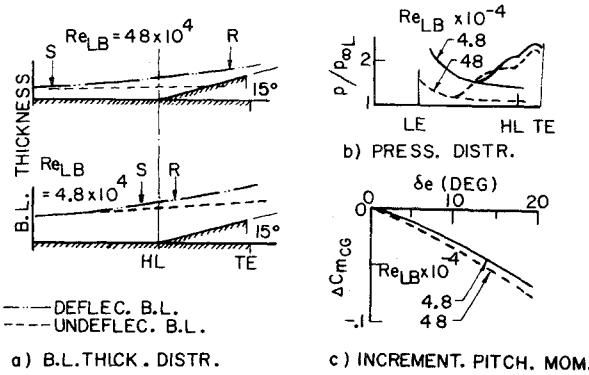

Fig. 11 Effects of Reynolds number on elevon effectiveness ($M_\infty = 15$, $\alpha = 20$ deg, $M_{\infty L} = 4.5$, $\gamma = 1.4$, $S_w = 0$).

For example, the qualitative trend of the upstream propagation of the separation point with increasing unit Reynolds number has been observed experimentally (see Fig. 4) when the deflected surface is infinitely long ($\delta/l_F \sin\delta_e \ll 1$) and most of the surface is exposed to the oncoming inviscid flow. In this case, the maximum pressure loading on the surface approaches the pressure as determined by the inviscid oblique shock theory. The thickness of the unperturbed laminar boundary layer at the hinge line decreases with increasing unit Reynolds number (but below transitional) and, in turn, larger longitudinal pressure gradients (dp/dx) near the hinge line are produced which aid the separation mechanism. The sample comparison is shown in Fig. 10. A thinner undisturbed boundary layer is produced by the flow with higher Reynolds number, and hence a larger portion of the deflected elevon surface is exposed to the inviscid stream at the instance of deflection. A larger separation area is produced for the larger Reynolds number, as observed in the pressure distributions, resulting in a less effective elevon, as indicated in the incremental pitching moments.

If the deflected surface has a finite chord length, the foregoing qualitative argument becomes only partially applicable. For example, the deflected control surface becomes ineffective, as it will eventually be submerged in the thickening unperturbed boundary layer with decreasing unit Reynolds number ($\delta/l_F \sin\delta_e > 1$), as shown in Fig. 11. Although the lower Reynolds number induces the smaller separated region, the incremental pitching moment trend is reversed from the previous example, with the elevon becoming more effective for the larger Reynolds number.

Wall Cooling Effects

It has been observed that viscous interaction produces a forward movement of the center of pressure due to upstream propagation of the separated region and reduces the degree of pressure recovery on the finite-length control surface with

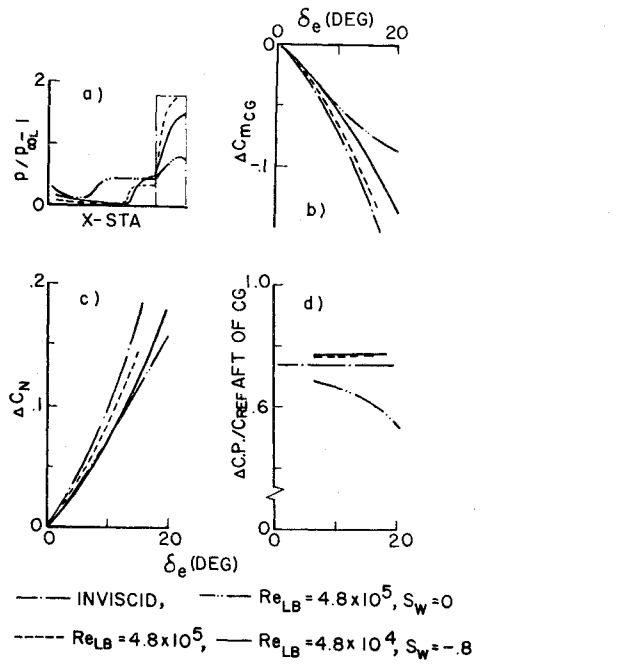

Fig. 12 Effects of wall cooling on elevon effectiveness: a) pressure distributions on wing midspan; b) incremental pitching moment coefficients; c) incremental normal force coefficients; d) incremental center-of-pressure shift.

increasing flap deflections. In some cases, one phenomenon predominates, and in others, a combination of both phenomena causes a degradation in aerodynamic control efficiency, depending upon the degree of wall cooling as compared to the freestream total enthalpy. For example, viscous interaction of flow over an adiabatic wall (Fig. 12: $S_w = 0$, $Re_{LB} = 4.8 \times 10^5$) produces a large forward movement of the separated region with respect to increasing elevon deflections but with much lower pressure recovery on the elevon surface than for ideal inviscid flow. Consequently, the forward shift of the center of pressure forces the recoverable pitching moment derivative ($dC_{mCG}/d\delta_e$) to become less negative. This is highly undesirable because control effectiveness degrades with respect to increasing surface deflection. Therefore, no additional aerodynamic control power beyond the limit is gained by increasing surface deflections.

For flow with high separation impedence (highly cooled wall, $S_w = -0.8$), the contribution arising from the separated region is overshadowed by the magnitude of pressure loadings on the control surface. Hence, very small center-of-pressure shifts occur with respect to varying deflection angles. Consequently, the pitching moment variation becomes proportional to the normal force variation. Although the magnitude of the recovery moment is degraded from the ideal inviscid value, depending upon the magnitude of Reynolds number, a trend of increasing control effectiveness with respect to increasing deflection angles is established. This condition poses no control reversal threat, and the loss of control effectiveness can be compensated for by a further increase in control deflection. For nonadiabatic flow with a moderately cooled wall, the combination of large movement of the separated region and a change in pressure distribution on the deflected surface could cause a degradation in control surface effectiveness.

The effect of wall cooling is very important when wind-tunnel test results are extrapolated to obtain vehicle flight aerodynamics. The present finding implied that the results of short-duration wind-tunnel/shock-tube tests (heated gas flow over a cold model) must be extrapolated with caution to vehicle flight conditions. The surface temperature of the

Orbiter (skin surface over the insulation tile) is expected to reach 2000-2500°F due to prolonged re-entry times of approximately 9 min. Therefore, viscous interaction of the flowfield on the flight vehicle may be enhanced, and control effectiveness may be reduced from the results indicated by short-duration wind-tunnel tests as the vehicle decelearates.

Spanwise Distributions of Peak and Plateau Pressures

As has been discussed in the foregoing sections, the viscous interaction phenomena on the finite-length compression surface are dictated by the Reynolds number at the hinge line (Re_{HL}), which is proportional to the forewing length, and the length of the deflection surface (l_F). Because of the double delta configuration of the Orbiter wing, the length ratio of the elevon (hinge line to trailing edge l_F) over the forewing (leading edge to hinge line l_w) increases in the outboard direction, with a maximum ratio of 0.35 reached at the wing tip.

In general, in the presence of strong viscous interactions, peak pressures on the control surfaces increase in the outboard direction, except near the wing tip, which is unpredictable. This is in concurence with the elevon/forewing length ratio distribution. Cooling of the wall and increasing of Reynolds number reduced the viscous interaction effect so that peak pressures on the elevon approach the value of the inviscid oblique shock loading.

Conclusion

Prediction of re-entry aerodynamic trim and control for a winged vehicle, such as the Space Shuttle Orbiter, can be made successfully with the application of a strip analysis of the vehicle planform, using the presently developed hypersonic laminar flow separation computer program. The present investigation has revealed that aerodynamic trim and control became more effective when a cooled surface was assured. The real-gas contribution effects of dissociation-recombination circuit of air molecules within the boundary layer on the flow separation mechanism is presently unknown and requires further investigation.

References

[1] Klineberg, J.M., "Theory of Laminar Viscous-Inviscid Interaction in Supersonic Flow," Ph.D. Thesis, California Inst. of Technology, Pasadena, Calif., 1968.

[2] Klineberg, J.M. and Lees, L., "Theory of Laminar Viscous-Inviscid Interactions in Supersonic Flow," *AIAA Journal,* Vol. 7, Dec. 1969, pp. 2211-2221.

[3] Lees, L. and Reeves, B.L., "Supersonic Separated and Reattaching Laminar Flows: I-General Theory and Application to Adiabatic Boundary Layer/Shock-Wave Interactions," *AIAA Journal,* Vol. 2, Nov. 1964, pp. 1907-1920.

[4] *Proceedings of the 1969 Symposium on Viscous Interaction Phenomena in Supersonic and Hypersonic Flow,* University of Dayton Press, Dayton, Ohio, 1969.

[5] Holden, M.S., "Theoretical and Experimental Studies of the Shock-Wave Boundary Interaction on Curved Compression Surfaces," *Proceedings of the 1969 Symposium,* (Ref. 4), pp. 213-270.

[6] Stollery, J.L., "Hypersonic Viscous Flow Over Concave and Convex Surfaces," *Proceedings of the 1969 Symposium,* (Ref. 4), pp. 181-212.

[7] Ko, D.R.S., and Kubota, T., "Supersonic Laminary Boundary Layer Along a Two-Dimensional Adiabatic Curves Ramp," *AIAA Journal,* Vol. 7, Feb. 1969, pp. 289-304.

[8] Hung, C.M. and MacCormack, R.W., "Numerical Solutions of Supersonic and Hypersonic Laminar Compression Corner Flow," *AIAA Journal,* Vol. 14, April 1976, pp. 475-481.

[9] Carter, J.E., "Numerical Solutions of the Navier-Stokes Equations for the Supersonic Laminar Flow over a Two Dimensional Compression Corner," NASA TRR-385, July 1972.

[10] Georgeff, M.P., "Momentum Integral Method for Viscous Interaction with Arbitrary Wall Cooling," *AIAA Journal,* Vol. 12, Oct. 1974, pp. 1393-1400.

[11] "Orbiter Aerodynamic Design Data Book," Space Div., Rockwell International, SD 72-SA-0060-1G, 1974.

[12] Gentry, A.E. and Smyth, D.N., "Hypersonic Arbitrary-Body Aerodynamic Computer Program, Mark III Version, Vol. II, Program Formulation and Listings," Douglas Rept. DAC 61552, April 1968, pp. 87-98.

[13] Karger, W.J. and Bonner, E., "Estimation of Hypersonic Aerodynamic Characteristics of Lifting Vehicles, Part IV: Control Effectiveness," Los Angeles Div., North American Aviation, NA6-271, June 12, 1967.

[14] Chapman, D.R. and Rubesin, M.N., "Temperature and Velocity Profiles in the Compressible Laminar Boundary Layer with Arbitrary Distributions of Surface Temperature," *Journal of the Aeronautical Sciences,* Vol. 16, Sept. 1949, pp. 547-565.

[15] Stewartson, K., "Correlated Incompressible and Compressible Boundary Layers," *Proceedings of the Royal Society (London),* Ser. A., Vol. 200, No. A1060, 1949, pp. 84-100.

[16] Cohen, C.B., and Reshotko, E., "Similar Solutions for the Compressible Laminar Boundary Layer with Heat Transfer and Pressure Gradient," NACA Rept. 1293, 1956.

[17] Rakich, J.V., "Introduction to the Proceedings of the Symposium of Computational Fluid Dynamics," *Proceedings of the AIAA Computational Fluid Dynamics Conference,* Palm Springs, Calif., July 19-20, 1973.

[18] Lewis, J., Kubota, T., and Lees, L., "Experimental Investigation of Supersonic Laminar, Two Dimensional Boundary Layer Separation in a Compression Corner With and Without Cooling," *AIAA Journal,* Vol. 6, Jan. 1966, pp. 7-13.

[19] Bloy, A.W. and Georgeff, M.P., "The Hypersonic Laminar Boundary Layer near Sharp Compression and Expansion Corners," *Journal of Fluid Mechanics,* Vol. 63, 1974, pp. 431-447.